To the Graduate Council:

I am submitting herewith a thesis written by Shahab Hatamtabrizi entitled "A Finite-Element Thermal Analysis of an Electroslag Casting Process." I recommend that it be accepted in partial fulfillment of the requirements for the degree of Master of Science, with a major in Engineering Science.

Bruce R. Dewey

Bruce R. Dewey, Major Professor

We have read this thesis and recommend its acceptance:

Accepted for the Council:

Vice Chancellor
Graduate Studies and Research

A FINITE-ELEMENT THERMAL ANALYSIS OF AN ELECTROSLAG CASTING PROCESS

A Thesis

Presented for the

Master of Science

Degree

The University of Tennessee, Knoxville

Shahab Hatamtabrizi

December 1981

ACKNOWLEDGEMENT

The author wishes to express special appreciation to his advisor, Professor Bruce R. Dewey, for his unlimited guidance and suggestions which contributed to this thesis.

The author also deeply acknowledges Dr. M Parang and Professor J. E. Stoneking, who served on the graduate committee and assisted in the review of the manuscript.

Special thanks are due to Professor J. E. Akin, who provided helpful insight into the use of the PAFEC code. The continuing support of the Department of Engineering Science and Mechanics, headed by Dr. William T. Snyder, is gratefully acknowledged.

Gratitude is expressed to the Welding Laboratory of the Metals and Ceramics Division of the Oak Ridge National Laboratory for the financial support of this thesis.

The able typing and other assistance in many ways given by Ms. Eunice Hinkle is very much appreciated.

Above all, the author expresses his deepest appreciation to his parents, Mr. and Mrs. Hatamtabrizi, for their encouragement, financial support and enthusiasm throughout his college education.

ABSTRACT

To aid in the design and development of equipment for the electroslag casting of graded-composition transition spool pieces, a finite element model has been developed. This model encompasses the electrode, slag, molten metal, solidified ingot, skin layer, and mold wall.

Solution of the electrical potential problem in the slag region gives the volumetric heat generation due to resistance (or joule) heating. Then, a heat transfer model is used to solve the conduction equations, with convection in the molten slag and molten metal treated by the use of effective conductivity valves. Several detailed features of the electroslag casting process have been taken into account, including the transport of heat from the slag to the molten metal by metal droplets. Predictions are made of temperature distribution as related to the metal pool profile, input power, properties and amount of slag, and other geometrical factors.

A parametric study on the effect of electrode penetration depth shows that power consumption and slag temperature increases as the electrode becomes nearer the metal pool. The temperature profile in the mold wall may be used to measure slag depth, location of the metal pool and other geometrical factors. Thus, control information is available from the wall temperature distribution.

Results developed in this study favorably agree with those from a prototypic collar mold operated at the Oak Ridge National Laboratory. Extension of the analysis techniques developed here appears feasible for development of the process for casting hollow ingots.

TABLE OF CONTENTS

LIST OF FIGURES

FIGURE PAGE

1. INTRODUCTION AND BACKGROUND

In many power plants, welded joints between dissimilar metals have presented special problems. Such joints--referred to as transition joints--are used in applications such as connecting heat exchanger tubes to superheater tubes. A ferritic steel such as 2 1/4 Cr-1 Mo often is an economical choice for the heat exchanger, while the superheater requires an austenitic steel such as type 316 stainless. Difficulty in maintaining satisfactory service life of transition joints stems from differences in thermal expansion and in thermal conductivity of ferritic and austenitic steels.

Research into improvement of such joints has involved weld filler materials, weld-joint geometry, and so forth. Selected for the Clinch River Breeder Reactor plant in Oak Ridge, Tennessee is the trimetal transition joint. Here, the spool piece consists of 2 1/4 Cr-1 Mo pipe, ERNiCr-3 filler metal, alloy 800H pipe, 16-8-2 filler metal, and type 316 stainless steel pipe. This sequence of materials was selected to provide a series of smaller steps of properties gradation.

Analysis and tests on the trimetal transition joint show problems still remain. The areas of trouble are where there are sudden composition changes. The 2 1/4 Cr-1 Mo heat-affected zone seems to be the "weakest link" in this transition.

A graded-composition transition joint is one possible alternative to welded transition joints. The gradation of composition can be planned to give a gradual change in properties between the 2 1/4 Cr-1 Mo steel and the type 316 stainless steel. While the idea at first looks very attractive, there are two problems that need to be addressed: (1) How can such a joint be fabricated? (2) Are the continuous spectra of alloys produced suitable from the standpoint of strength, corrosion resistance, and other service-related factors? The fabrication question is partially addressed in this report. The suitability of transition joints with graded composition is left for future research.

The electroslag casting (ESC) process has been selected as a possible fabrication method. Here the feed stock, or consumable electrode, is made of the desired alloys, spliced together. As the electrode is melted, some mixture occurs in the metal pool and a graded composition results. The slag bath tends to purify the resulting ingot.

Casting solid ingots is much more straightforward than casting hollow ingots. It was decided to use a collar mold, whereby the ingot is continuously withdrawn from the bottom of the mold as the electrode is fed into the top. Besides casting solid ingots, the collar mold has the capability of casting hollow pipe of some limited length with a core-piece protruding up just into the molten metal pool. With this type of casting system for hollow ingots, it is important to maintain the metal pool in exactly the right position.

Up to the present time, however, work has been limited to systems for producing solid ingots which incorporate the control functions to render the possible casting of hollow ingots. In a prototypic system demonstrated at Oak Ridge National Laboratory (ORNL), the controlling minicomputer interrogates a system of thermocouples imbedded in the wall of the copper mold, Figure 1. This system has been designed to provide information on the location of the molten metal pool. Testing[1] at ORNL has shown efficient and accurate control of this location. Possibly

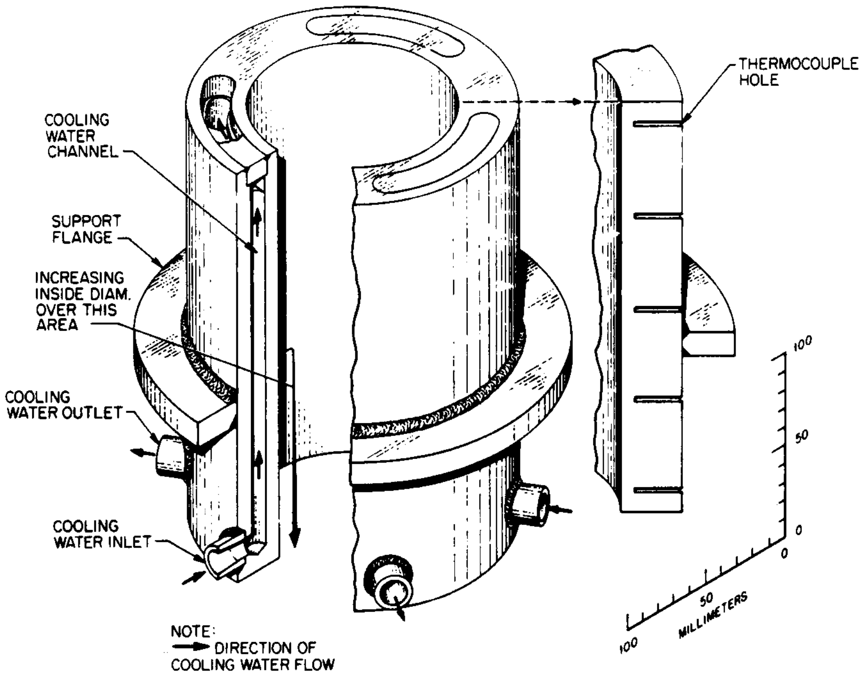

Figure 1. Cross Sectional View of Water-Cooled Copper Mold for Casting Transition Ingots. The Thermocouples are Used for Control Information.

other information is available from the thermocouple temperatures besides the location of peak temperature.

The analysis presented here looks at detailed heat transfer considerations. This is an attempt to answer the question about obtaining more information concerning control of the casting process. In particular, the copper wall of the mold has been included in the analysis so that we can study the effect of variables such as the depth of the slag bath and electrode penetration depth.

2. DESCRIPTION OF ELECTROSLAG PROCESS

Operation

The electroslag remelting and casting processes (ESR and ESC) have been in general use for a long while. These processes are attractive because chemical refining is done through a slag of controlled composition and solidification can be adequately controlled. Illustrated in Figure 2 is a typical electroslag casting setup. In this process, the electrical energy is changed to thermal energy through resistance or joule heating of the slag. The consumable electrode (melting material) is suspended in the slag which is contained in a water-cooled copper mold. A high-amperage, low-voltage power supply is connected to the electrode which serves as one pole and the base plate which serves as the other pole. The temperature in the slag rises above the melting temperature of the electrode; metal droplets melt off the tip of the electrode and traverse the slag and form a metal pool.

Slag

The slag which is used to generate heat not only refines the metal but also protects the metal from reaction oxidation with the atmosphere. The slag must have suitable electrical resistivity to generate heat and must have stable liquidus ranges at high temperatures (1400 °C - 2000 °C). The chemical and electrochemical reactions can be controlled by the composition of the slag. The most common slag compositions used are CaF_2 + Al_2O_3 + CaO or MgO. Commercial slags have various other components which result in various special characteristics. These commercial slags are chosen by experience.

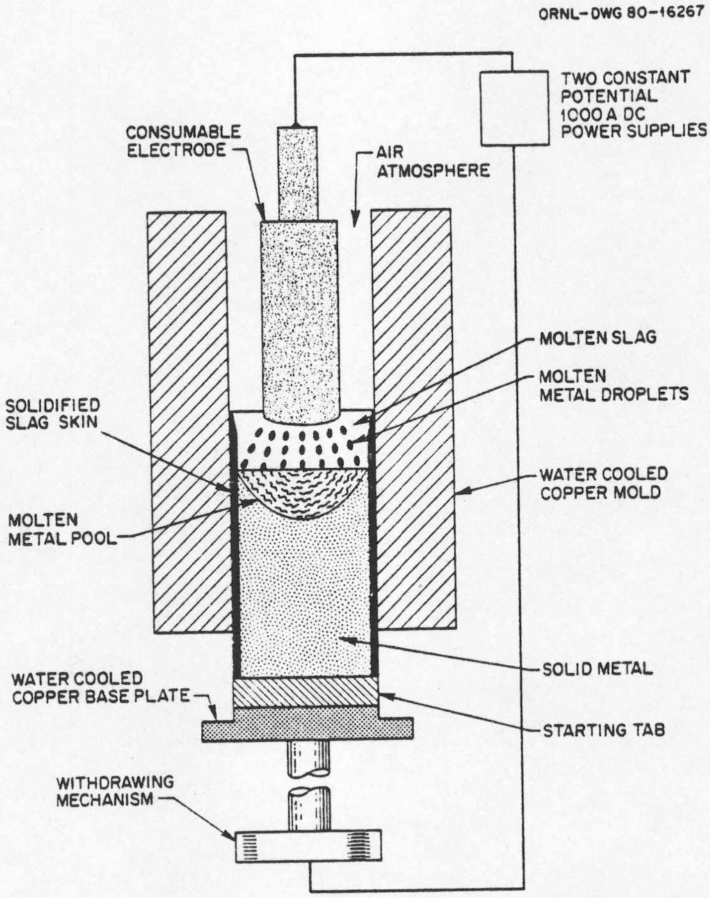

Figure 2. Collar Mold for Electroslag Casting as Implemented at ORNL[1]

Since the melting temperature of the slag is below that of metal, a solid slag skin layer forms at the inner surface of the mold due to heat removal through water channels. This skin and subsequent air gap formation create a thermal barrier around the ingot. Also, the slag skin, which is on the order of a few millimeters thick, provides electrical insulation around the ingot causing the current to travel down to the base plate through the ingot. According to Stenzel and Thomas[2] only a few amperes to milliamperes of current, depending on the composition of slag and type of cooling system, go through the slag skin to the mold wall. This amount of current is negligible when compared to thousands of amperes used in this process. This high resistance of the slag skin is due to the dependency of electrical conductivity of slag on temperature.

The electrical resistivity of the slag is orders of magnitude times higher than that of metal. For this reason joule heat generation in the electrode and ingot is negligible compared to that in the slag.

Fluid Flow and Heat Transfer

The fluid motion in ESR process is caused by electromagnetic forces and by buoyancy (due to temperature gradients) forces. The electromagnetic forces result from the vector product of current density and magnetic flux density. The electromagnetic forces that cause flows are due to the nonuniform distributions of current density and magnetic flux density. The electromagnetic force is the major driving force[2] and it either couples with buoyancy force or counters it, depending on the polarity of input power. In general, the nature of flow is turbulent as reported in literature.[3-8]

The convection heat transfer in the slag and metal, as well as fluid motion, have an important effect on refining process and have been studied by many investigators.[4-9] The metal droplets are superheated as they descend through the slag. Phase-change heat transfer takes place at the electrode tip (melting) and the mushy zone (solidification). At the slag-free surface, radiation heat transfer takes place between the slag-free surface, electrode, mold wall, and atmosphere. There is also radiation heat transfer through air gaps of slag skin layer. This has been studied by Maulvault.[11] Heat transfer in other parts is by conduction except at the cooling water channels where heat is removed by forced convection.

Other aspects of the electroslag refining or casting process such as the electrical properties or chemical aspects of refining metal are not important in this work. Duckworth and Hoyle[12] describe the fundamentals.

3. REVIEW OF PREVIOUS WORK

There are numerous publications concerning the electroslag refining (ESR) process. Several mathematical models have been developed to model temperature distribution and fluid flow in the ESR process. These models have attempted to explain and predict the physical phenomena happening in this process in order to obtain better understanding and control. In this chapter, the major mathematical models developed to represent this process are discussed in two major categories along with some of the effort made in controlling this process.

The first group of models[11,13-21] are earlier ones which represent only the molten metal and solidified ingot. The slag-metal interface was represented either by a line of constant temperature or by heat flux representing the molten slag. The convection in the metal pool was accounted for by using the effective thermal conductivity value and the melt rate was an input parameter to these models. The distinctions among these models were the boundary conditions and the method used in modeling the solidification process and whether or not they were steady-state.

These metal/ingot models were able to explain the effect of melt rate and metal pool conductivity on temperature distribution. They also helped to establish boundary conditions for the ingot and provided extensive experimental results as well. Such models were not able to predict and relate the location and shape of metal pool to the input parameters such as input power, geometry, and amount and composition of slag used. This inability was due to the fact that these models did not include the slag and the electrode. A comprehensive review of some of these models is presented by Ballantyne and Mitchell.[21]

The second category[4-9] are the more recently developed models which were based on more fundamental principles. These models included the physical phenomena happening in the slag through Navier-Stokes equations and Maxwell's equations. The basic and common approach taken here is:

1. Current profiles are calculated for an assumed shape of the melting electrode tip.

2. Fluid flow equations are solved for the velocity distribution, considering both the electromagnetic and thermal convective (buoyancy) body forces.

3. Heat transfer equations are solved for temperature distribution.

4. The convection process in the metal pool is incorporated in the model using effective values of thermal conductivity.

Some investigators assumed conical[9] and some, cylindrical[4-8] melting electrode tip shapes. Kreyenberg and Schwerdtfeger[8] assumed the temperature distribution at the slag-metal interface, because they considered the fluid flow and heat transfer in the slag phase only. Others considered both the slag and metal phases. Dilawari and Szekely[4-6] and Choudhary and Szekely[7] considered the heat transfer between the slag and the falling metal droplets as well as considering the turbulent nature of the flow. All of these investigators except Choudhary and Szekely[7] postulated the metal pool shape and ignored the heat transfer in the ingot. Thus currently, the model developed by Choudhary and Szekely[7] is probably the most comprehensive one.

So far all of these models have excluded the mold wall. Joshi and Mitchell[22] experimentally studied the mold wall through embedding thermocouples in the wall. They reported a parabolic temperature and flux distribution in the mold wall of an ESR system.

Recently, Oak Ridge investigators[1,28] assumed the temperature distribution in the wall could be used for control purposes. Through embedding thermocouples in the wall and using the assumption of a parabolic temperature distribution in the wall (in the plane of thermocouples) they implemented an algorithm to locate the slag-metal interface during the run. They obtained good agreement with experimental results on a dynamic laboratory scale mold. This work to some extent shows the feasibility of using the mold wall temperature distribution for control purposes.

The present work is an effort toward studying the temperature in the mold wall through developing a predictive heat transfer model. This model related the mold wall temperature distribution and the metal pool shape to the imput parameters such as input power, electrode penetration depth, dimensions of mold and electrode, amount and composition of slag used.

4. MATHEMATICAL MODELING

The finite element models developed to represent the heat generation and heat transfer phenomena are presented in this chapter. Also, the assumptions made in modeling and the governing equations are described.

Assumptions

The main assumptions made in the present model are listed and discussed in this section. Other assumptions will be discussed in the appropriate places of this chapter.

1. Axisymmetric geometry is assumed. The six vertical water-cooling channels spaced evenly around the wall of the mold modeled in this work deviate from the axisymmetric assumption. The excellent conductivity of the copper wall is assumed to mitigate this effect. The consideration of this effect would involve the solution of a three-dimensional model. The marginal improvement in the accuracy of the results definitely would not justify the expensive undertaking of the three-dimensional solution.

2. A quasi-steady state is assumed, since no parameters vary rapidly with time during normal operation.

3. Slag-electrode and slag-metal boundaries are modeled as cylindrical flat surfaces. This is reasonable considering the slag as a liquid, conforming to the shape of the container.

4. The effect of convection due to magnetic and buoyancy forces in the slag and metal phases are taken into account by the use of effective values of thermal conductivity. This approach of representing the

convection effects has been used in the electroslag literature.[23] Based on a study of the convection process in the slag and metal pool, Choudhary and Szekely[7] reported effective thermal conductivity values of 1.7 to 4.5 times the atomic thermal conductivity of the metal as reasonable for the metal pool phase. Roy et al[23] studied the relationship between effective thermal conductivity of the slag and temperature distribution. Their suggestions were considered in choosing the appropriate value of this parameter for the present work.

5. The electrical conductivity of the slag is assumed to be uniform. Neglecting the temperature dependency of the electrical conductivity of the slag will not result in appreciable changes.[23]

6. The chemical and electrochemical reactions, and the subsequent effects are not considered. Endothermic and exothermic electrochemical reactions must affect the energy balance. The amount of energy is not known due to the lack of data on the reactions that take place, and it is felt that the quantity of heat is not large.

7. The mold wall is assumed to be electrically insulated due to the presence of the slag skin layer at the inner surface of the mold. According to Stenzel and Thomas[2], current mainly flows in through the electrode and out through the base plate.

8. Since the electrical resistivity of the slag is orders of magnitude greater than that of metal, all joule heating is assumed to be in the slag phase.

9. Melt rate is an input parameter to this model. It is more direct to assume the melt rate than it is to calculate it from the heat balance of the process.

10. Heat transfered from the slag-free surface (top of slag) to the mold wall, electrode, and atmosphere is neglected. This process is free convection and radiation, which is assumed to be an order of magnitude less than the conduction transfer between solid surfaces.

11. Direct DC input power is assumed. This is to enable use of data developed by previous workers[2,3] for effective thermal conductivity in the presence of magnetic effects.

Heat Generation

In order to obtain the local distribution of heat generation, first the voltage distribution should be found. As stated before, the voltage drop is assumed to be across the slag phase only. The voltage distribution is obtained through the solution of Laplace's equation

$$\vec{\nabla}\cdot(\sigma\vec{\nabla} V) = 0 \tag{1}$$

where:

σ is the electrical conductivity of the slag in $(\text{ohm} - \text{m})^{-1}$

V is the potential in volts

and the electric field $\vec{E}$(V/m) is

$$\vec{E} = -\vec{\nabla}V \tag{2}$$

The current density $\vec{J}$(A/m^2) is obtained through the Ohm's law

$$\vec{J} = \sigma\vec{E} \tag{3}$$

And finally the local value of volumetric heat generation rate $\dot{q}_V$(w/m^3) is

$$\dot{q}_V = \vec{J}\cdot\vec{E} \tag{4}$$

The local heat generation rate $\dot{Q}_g$(w) is the product of $\dot{q}_V$ and the local volume.

In the solution of equation (1) for the voltage distribution, the following boundary conditions are used:

1. Slag-metal interface: $V = 0$

2. Electrode surface: $V = V_{e\ell}$

where $V_{e\ell}$ is the applied voltage in volts.

3. Mold wall: electrically insulated mold wall due to the presence of slag skin layer

$$\frac{\partial V}{\partial r} = 0 \quad (r, \theta, x \text{ are cylindrical coordinates})$$

4. Slag-atmosphere: $\frac{\partial V}{\partial x} = 0$

Heat Transfer Equations

As stated before, the effect of the motion of the slag and metal phases on temperature distribution is taken into account by the use of effective values of thermal conductivity. Therefore, the mathematical statement of the problem reduces to a set of conduction heat transfer equations which are of the following form:

$$\vec{\nabla}\cdot(K_i\vec{\nabla}T) + \dot{Q}_i/VOL_i = 0 \tag{5}$$

where VOL_i is volume of region i, $\dot{Q}_i$ is the heat source rate (w) in region i and is zero everywhere except at the slag, mushy zone, and metal phases, and K_i is the effective thermal conductivity in i.

At the mushy zone $\dot{Q}_i$ is equal to $\dot{Q}_{fu}$, the rate at which heat is given off due to the solidification of metal, calculated as follows:

$$\dot{Q}_{fu} = (\Delta H)\,\dot{m} \tag{6}$$

Here

ΔH is the latent heat of fusion of metal in J/Kg.

$\dot{m}$ is the melt rate in Kg/s.

At the metal phase $\dot{Q}_i$ is equal to $\dot{Q}_{md}$, the rate at which heat is taken away from the slag by the metal droplets as they traverse the slag. This power is dissipated by the metal droplets in the area under the electrode in the metal pool. Its magnitude is

$$\dot{Q}_{md} = \dot{m}\ C_p\ \Delta T \tag{7}$$

where

ΔT is the temperature gain of the metal droplets as they traverse the slag.

C_p is the specific heat of the metal droplets.

At the slag phase $\dot{Q}_i$ is the result of (i) the spatially distributed joule heat generation rate, (ii) the rate of energy removal by the metal droplets ($-\dot{Q}_{md}$) from the slag volume under the electrode, (iii) rate of energy taken away from the slag due to the melting of the electrode (Q_{Fu}) tip, and (iv) the rate of energy consumption in heating the electrode ($\dot{Q}_{e\ell}$) from room temperature (T_{room}) to its melting temperature ($T_{\ell m}$) which is calculated as follows:

$$\dot{Q}_{e\ell} = \dot{m}\ C_p\ (T_{\ell m} - T_{room}) \tag{8}$$

Statement of the boundary conditions and the descriptions of the thermal model is deferred until the finite element discussion.

Finite Element Modeling

All the finite element computations and graphics were performed with PAFEC[27] -- Programs for Automatic Finite Element Calculations. The program is a large, general purpose code which performs stress analysis, dynamics, creep, plasticity, heat transfer, and other potential field problems.

An axisymmetric finite element model of the process is shown in Figure 3. The column of elements on the right shows convection elements which model the cooling water channels and heat loss to the surrounding atmosphere. The next two columns of elements represent the copper mold wall. Next to the mold wall are two columns of elements which represent the solid slag skin layer and the air gaps. The slag phase and the mushy zone are shown shaded for illustration purposes. The molten metal phase is located between the two shaded zones. The bottom row of elements are convection elements which represent the heat loss from the base plate. The zone of elements above that represent the solidified ingot. The electrode immersed in the slag is modeled in the upper left of the mesh.

Quadrilateral and triangular conduction heat transfer elements were used in modeling the slag, electrode, molten metal, mushy zone, solid ingot, skin layer, and mold wall. All elements were isoparametric with quadratic interpolation functions. The isoparametric elements help to model the irregular geometry of the system. An average of 370 elements with an average of 1150 nodes were used in the mesh. These nodes each have one degree of freedom (temperature).

In finite element modeling of heat transfer problems, the outside boundary of the system should be specified either by temperature or flux. In PAFEC, the default is the insulated boundary condition. The outside boundary of convection elements (the right and lower boundaries as shown in Figure 3) are assigned the cooling water temperature (t_W). The center line is taken as insulated boundary due to the symmetry of the problem. Heat transfer to the atmosphere from the free slag surface, the top of

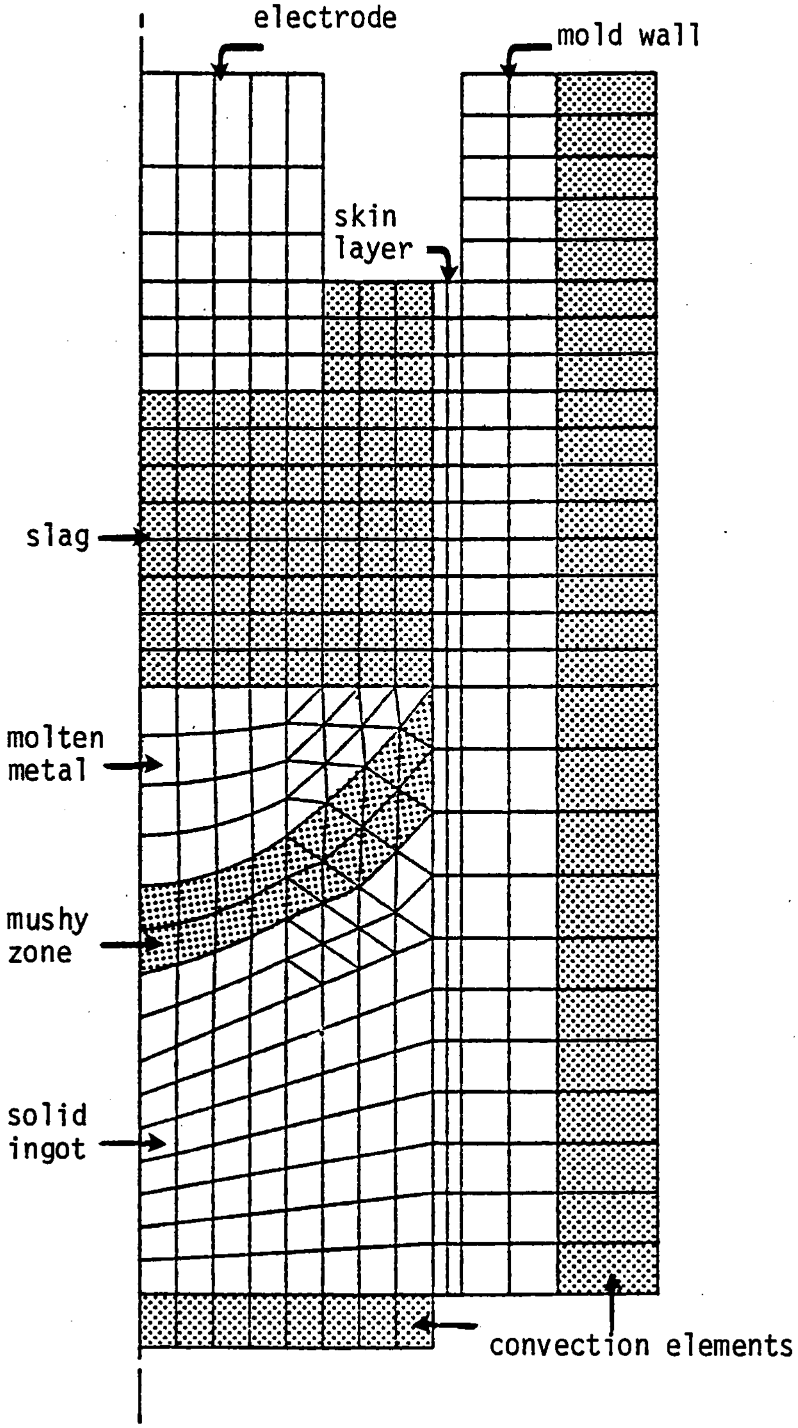

Figure 3. The Axisymmetric Mesh Generated for the Thermal Model

the mold wall and the electrode surface are assumed to be much smaller than to the mold; these boundaries are assumed to be insulated.

Only a few centimeters of the electrode are modeled and the end of the electrode is assumed to be insulated. According to the experimental investigation of Maulvault[11], approximately adiabatic heat flow conditions exist on the surface of the electrode just above the slag level. Melting is assumed to take place at the tip of the electrode and for this reason the melting temperature of the metal is assigned to the tip of the electrode. The molten slag--skin layer interface is assigned the melting temperature of the slag ($T_{\ell s}$), because of the solidification of the slag next to the cooling wall.

As discussed before, the calculation of the spatial distribution of heat generation requires knowledge of the voltage distribution. A finite element model similar to the thermal model has been developed to represent the voltage distribution in the slag. Figure 4 shows the axisymmetric mesh generated. Since the electrical field equations have the same form as the heat transfer equations, conduction heat transfer elements can be used for the solution of the Laplace equation. Enough elements were used to properly model the voltage gradient across the slag phase. An average of 70 elements (average of 250 nodes) were used for each different operating condition. The boundary conditions for this model have been discussed previously.

With voltage distribution known, the current density and the volumetric heat generation were found at every node. Special algorithms were developed to multiply the volume surrounding every node by the volumetric heat generation term to obtain the input flux ($\dot{Q}_g$) (in watts) to the thermal model.

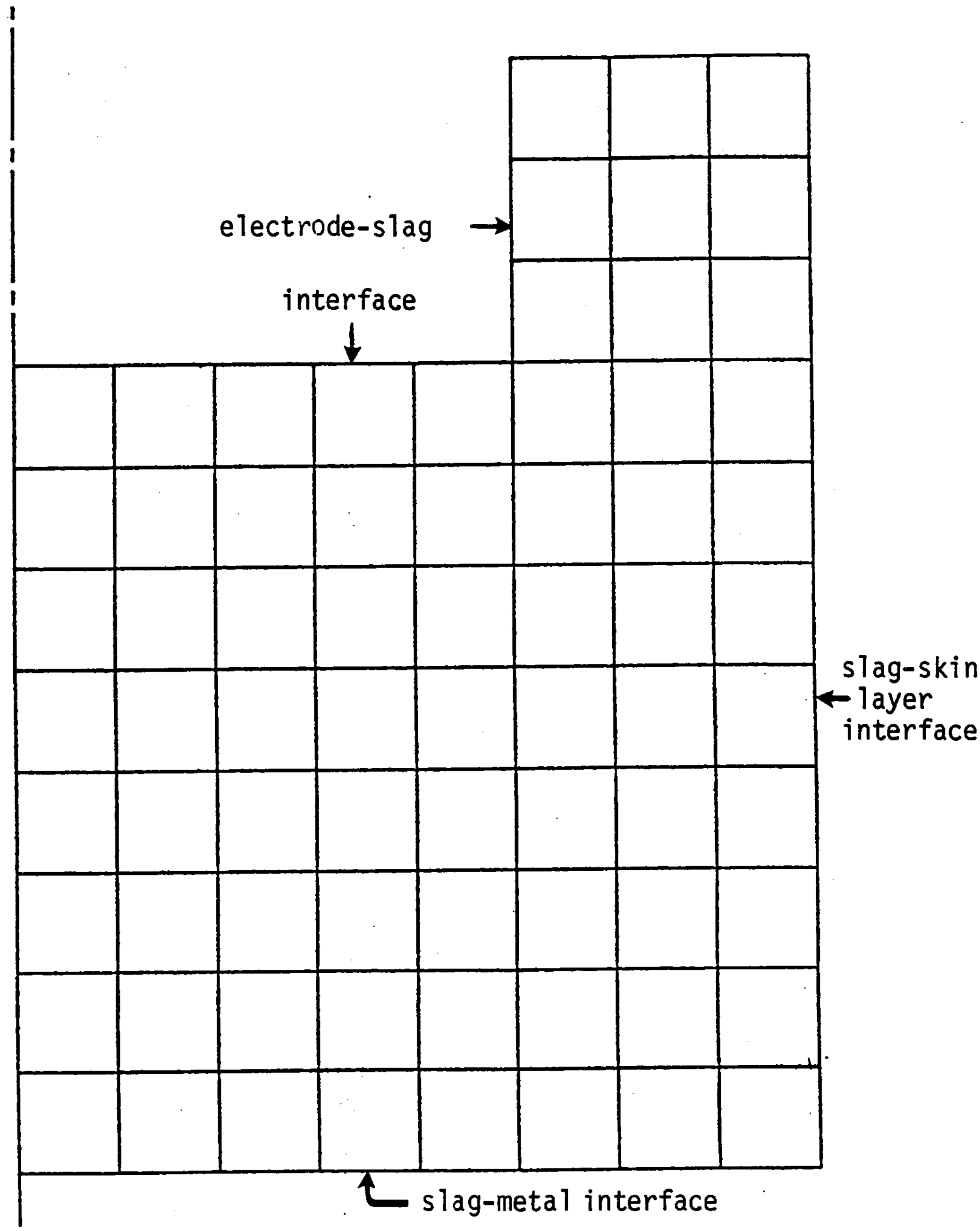

Figure 4. The Axisymmetric Mesh Generated for the Calculation of Voltage Distribution

Computational Detail

The flux terms $\dot{Q}_g$, $\dot{Q}_{fu}$, $\dot{Q}_{md}$ and $\dot{Q}_{e\ell}$ were distributed over the appropriate nodes, which, to be modeled consistently, require consideration of the element interpolation. For example, a uniform flux on the edge of an eight-noded quadrilateral element should have a relative weight of - 1/12 at the corner nodes and + 1/3 at the midside nodes. For six-noded triangular elements, the weights are - 1/3 at the corner nodes and +2/3 at the midside nodes. Special algorithms were developed to read the connectivity of the elements and do these calculations.

The DEC-10 computer and PAFEC[27] (Level 3) at The University of Tennessee Computing Center were used. A typical time for a complete run was on the order of 420 seconds using a region of 70K words. This figure includes the time used for the calculation of heat generation, and temperature calculation.

As a check on the accuracy of the results, an ASME-Sponsored Program Verification Library[29] was consulted. Since the elements used in the present work have a quadratic interpolation function while the reference[29] used linear interpolations, the computations are expected to be more accurate. The average discrepancy observed in the reference[29] was about 0.03%, depending on the number of elements used. The average gradient in the present work is above five times higher than that of the reference.[29] If it is assumed that the discretization error increases linearly with the gradient, the computations should not be off more than 0.15%. The irregular geometry and often unoptimum aspect ratios could increase this error up to 1.5%.

Physical Properties and Parameters Used

The geometry used for the computations are for a laboratory-scale mold used in the Metals and Ceramics Division Welding Laboratory at the Oak Ridge National Laboratory.[1] The dimensions of this mold and other dimensions are listed in Table 1. Physical properties and parameters used in the model are given in Table 2. In the computation method adopted here, constant properties were used, but allowance was made for the different thermal conductivity of the skin layer at different regions.

The properties of the metal are for pure iron and intermediate carbon steels. In casting transition ingots, there will be variable mechanical and thermal properties of the metal in the process. However, the properties of metals such as type 316 stainless steel, 2-1/4 Cr-1 Mo, etc. are of the same order as those of typical steels, and not greatly different. Thus, constant and typically average properties for the casting metal have been used. Typical properties were obtained from Choudhary and Szekely[7] and Elliot and Maulvault.[16] The properties of liquid slag as well as the melt rate were taken from Choudhary and Szekely.[7]

The thermal conductivities of the skin layer were obtained from the work of Maulvault[11] who studied the mechanism of heat transfer across the skin layer. He considered the radiation exchange across the air gaps as well as the conduction through the air gaps and solid slag crust. He reported heat transfer coefficients for these layers at the regions of solid ingot and metal pool. These heat transfer coefficients were divided by the thickness of the skin layer in order to obtain the thermal conductivity of the skin layer. The thickness of the skin layer as reported

TABLE 1

THE PHYSICAL DIMENSIONS OF THE MODEL

Detail	Dimensions
mold height	21.082 cm
mold interior radius	5.08 cm
mold wall thickness	1.693 cm
electrode radius	3.175 cm
distance between slag-metal interface and slag-atmosphere interface (slag height)	9.021 to 6.578 cm
distance between the base plate and slag-metal interface (ingot height)	10.541 cm
distance between the electrode tip and the slag-metal interface, b	1.905 to 5.715 cm
electrode penetration depth, a	7.11 to 0.863 cm
solid skin layer thickness	0.50 cm
ingot radius	5.08 cm

TABLE 2

PHYSICAL PROPERTIES AND PARAMETERS USED

Property or Parameter	Value
melting temperature of metal, $T_{\ell m}$	1450°C
solidus temperature of metal	1250°C
melting temperature of slag, $T_{\ell s}$	1377°C
room temperature, T_{room}	20°C
cooling water channel temperature, T_w	15°C
temperature gain of metal droplets, ΔT	103°C
thermal conductivity of solid ingot	0.3139 w/cm°K
thermal conductivity of electrode	0.3139 w/cm°K
thermal conductivity of mushy zone	0.3139 w/cm°K
effective thermal conductivity of slag phase	2.5116 w/cm°K
effective thermal conductivity of metal pool	1.2556 w/cm°K
thermal conductivity of skin layer at solid ingot	0.02204 w/cm°K
thermal conductivity of skin layer at metal pool	0.04268 w/cm°K
thermal conductivity of skin layer at slag phase	0.04659 w/cm°K
thermal conductivity of copper mold wall	3.7674 w/cm°K
voltage	40 volts
current	3.425 to 1.3 KA
electrical conductivity of slag,	2.50 mho/cm
density of slag	2.85×10^{-3} Kg/cm^3
specific heat of liquid metal	753 J/Kg K°
weight of slag	1.45 Kg
melt rate	10.13 to 13.38 g/s
latent heat of fusion of metal, ΔH	247 KJ/Kg
mold wall water channel heat transfer coefficient	0.9 w/cm^2°K
base plate heat transfer coefficient	4.18×10^{-2} w/cm^2°K

by Maulvault[11] is 0.9 mm. However, a thickness of 5 mm was used in the thermal model to avoid the distortion of the quadrilateral finite elements. The values of the thermal conductivities of the skin layer were adjusted to compensate the effect of unreasonable skin thickness. The skin layer at the molten slag phase was assumed to be composed of a solid slag crust only. The heat transfer coefficient across the solid slag crust was also taken from Maulvault[11] and was adjusted to compensate for the difference in thicknesses used.

The effective values of thermal conductivity depend on the atomic thermal conductivity values and convection associated with flow. The effective thermal conductivity value for the metal pool phase was estimated from the suggestions made by Choudhary and Szekely[7] and are in reasonable agreement with the values used by Ballantyne and Mitchell[21] and Roy et al.[23] The effective thermal conductivity of the slag phase was estimated from the work of Roy et al[23] who examined the effect of this parameter on temperature distribution.

The value of the heat transfer coefficient at the base plate was taken from the work of Ballantyne and Mitchell.[21] The heat transfer coefficient at the exterior of the mold wall, suggested by Maulvault[11] was tested in the model and resulted in unreasonably high temperatures. Therefore, this coefficient was adjusted in order to obtain more reasonable temperatures in the wall.

The temperature gain of the metal droplets was obtained from Dilawari and Szekely.[6] Their theoretical study of the mechanism of heat removal in the slag by metal droplets reported an average temperature gain of 103 °C.

5. RESULTS AND DISCUSSION

Typical computed results in the form of a parametric study done on the effect of the electrode penetration depth are now presented and discussed. The computations were performed for the electroslag collar mold[1] at the ORNL Metals and Ceramics Division. In the parametric study, the voltage, the amount, and the composition of the slag were kept constant, while the distance between the electrode tip and ingot (electrode penetration depth) was varied. The resulting effects on temperature distribution and heat generation were studied. The displacement of the free slag surface (boundary between the slag surface and the atmosphere) which results from changes in the electrode penetration depth was considered.

The results are presented in two sections, one for heat generation and the other for temperature distribution. The results are compared with the experimental and theoretical findings of others where possible. In the following discussions, the operating conditions refer to the conditions in Table 3.

Heat Generation

In Table 3 is shown the effect of electrode penetration depth on current consumption and heat generation. It is noted that as the electrode penetration depth increases, the power consumption (heat generation) increases too. This is due to the fact that less volume of slag is contained under the electrode causing lower resistance and higher current. This is intuitively obvious.

TABLE 3

RELATION BETWEEN ELECTRODE PENETRATION DEPTH AND INPUT POWER FOR OPERATING CONDITIONS 1 THROUGH 7

Operating Condition Number	Electrode Penetration Depth, a (cm)	Distance Between Electrode Tip and Ingot, b (cm)	Voltage (volt)	Current (ampere)	Input Power (kw)
1	7.116	1.905	40.0	3.425	137
2	6.074	2.54	40.0	2.675	107
3	5.03	3.175	40.0	2.2	88
4	3.99	3.81	40.0	1.875	75
5	2.95	4.445	40.0	1.625	65
6	1.905	5.08	40.0	1.45	58
7	0.863	5.715	40.0	1.3	52

As stated before, local values of voltage are needed for the calculation of heat generation. In Figures 5 and 6 are shown the voltage distributions for operating conditions 1 and 5 of Table 3, respectively. As observed in these figures, the voltage drop occurs mainly in the area under the electrode which causes most of the heat generation to take place there. Also, the contours near the slag-metal interface become more uniform which results in more uniform heat generation in this area. These are well in agreement with the theoretical findings of Choudhary and Szekely.[7] The difference between the operating conditions shown in these two figures results from the change in electrode penetration depth. Therefore, heat generation is very much affected by the geometry and it is to be noted that the assumption of a flat electrode melting tip must affect the heat generation intensity and temperature distribution.

In Figure 7 is shown a plot of nondimensionalized form of the results in Table 3. A least square curve fitting method was used to fit the data into a polynomial curve. The polynomial equation found suitable is:

$$\frac{Q_g}{Q_R} = 1.184 - 1.58x + 4.22x^2 \qquad (9)$$

$$x = \frac{a}{(a + b)}$$

$$0.2 \leq x \leq 1.0$$

where:

a = electrode penetration depth (Figure 8)

b = distance between the electrode tip and ingot

Q_R = reference input power, 52 Kw (40 V, 1.3 KA)

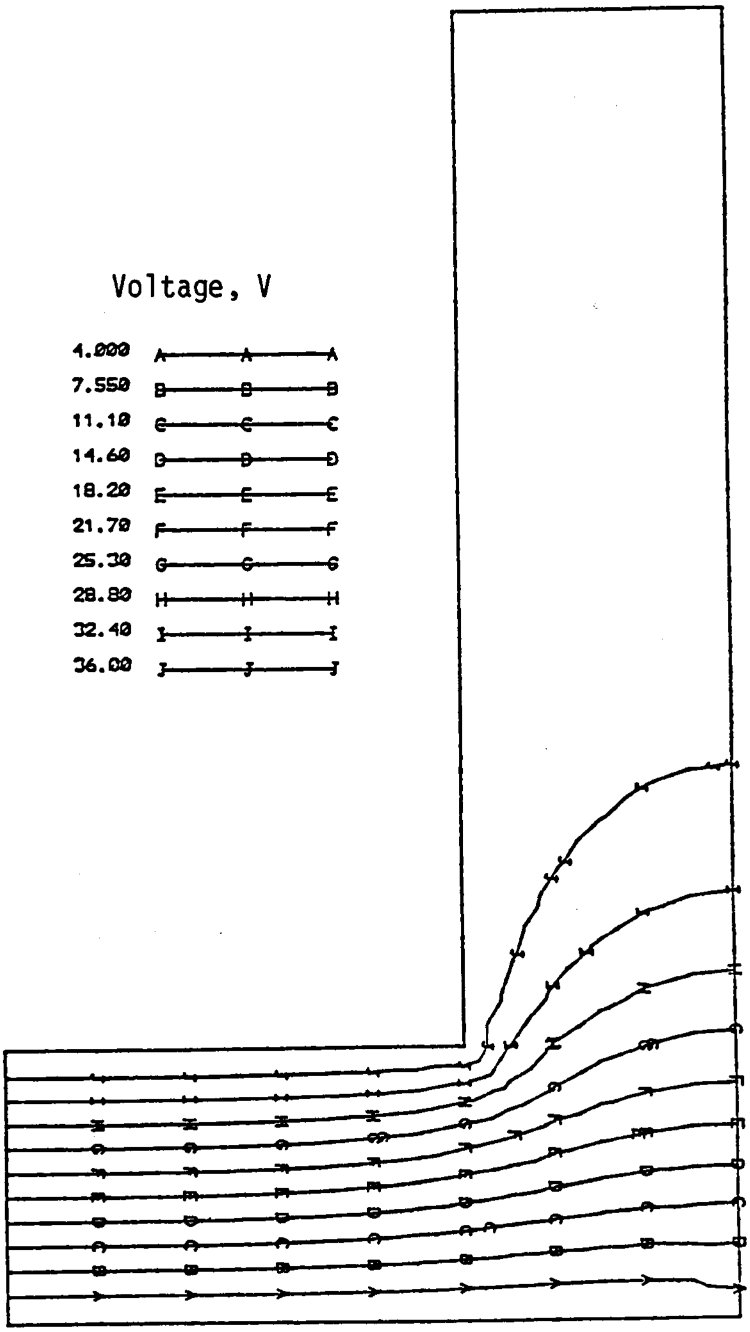

Figure 5. Voltage Distribution in the Slag for Operating Condition 1

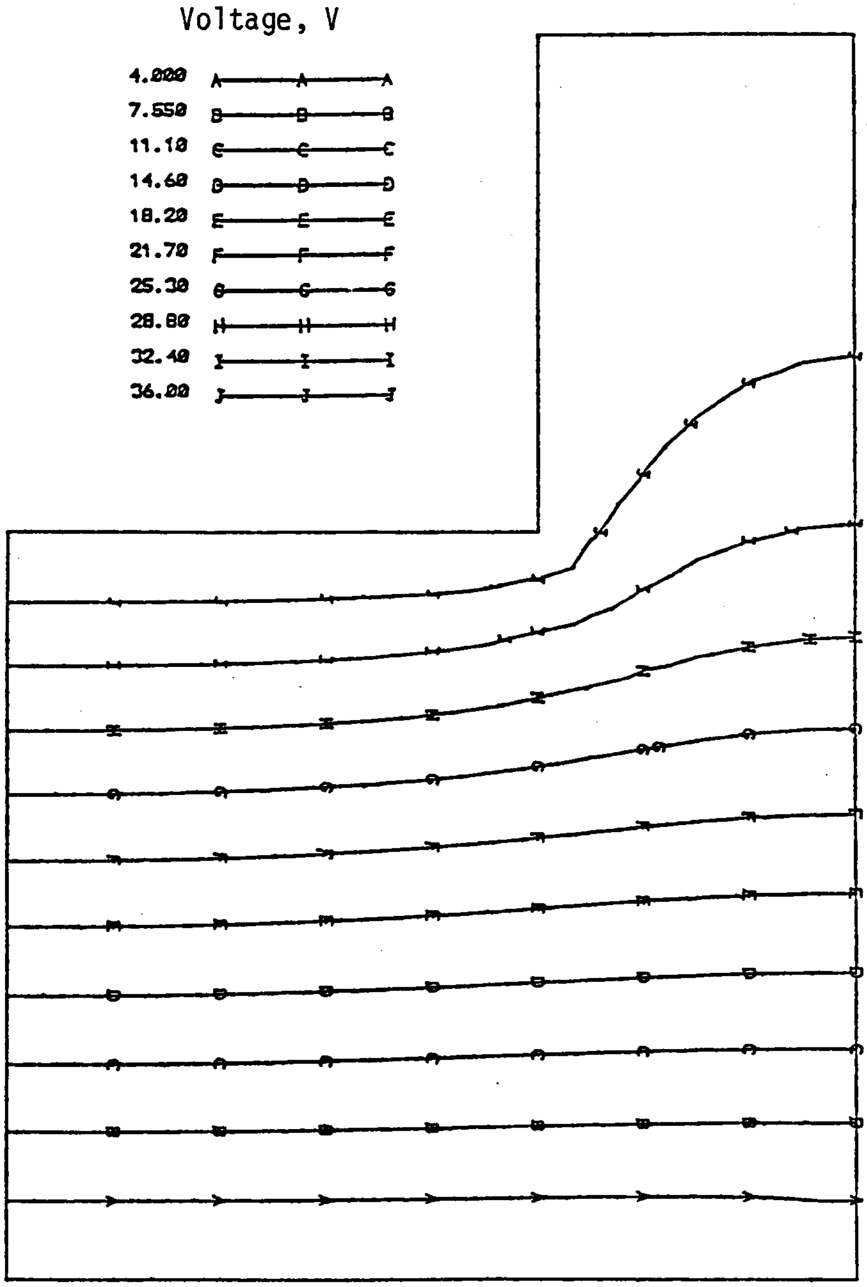

Figure 6. Voltage Distribution in the Slag
for Operating Condition 5

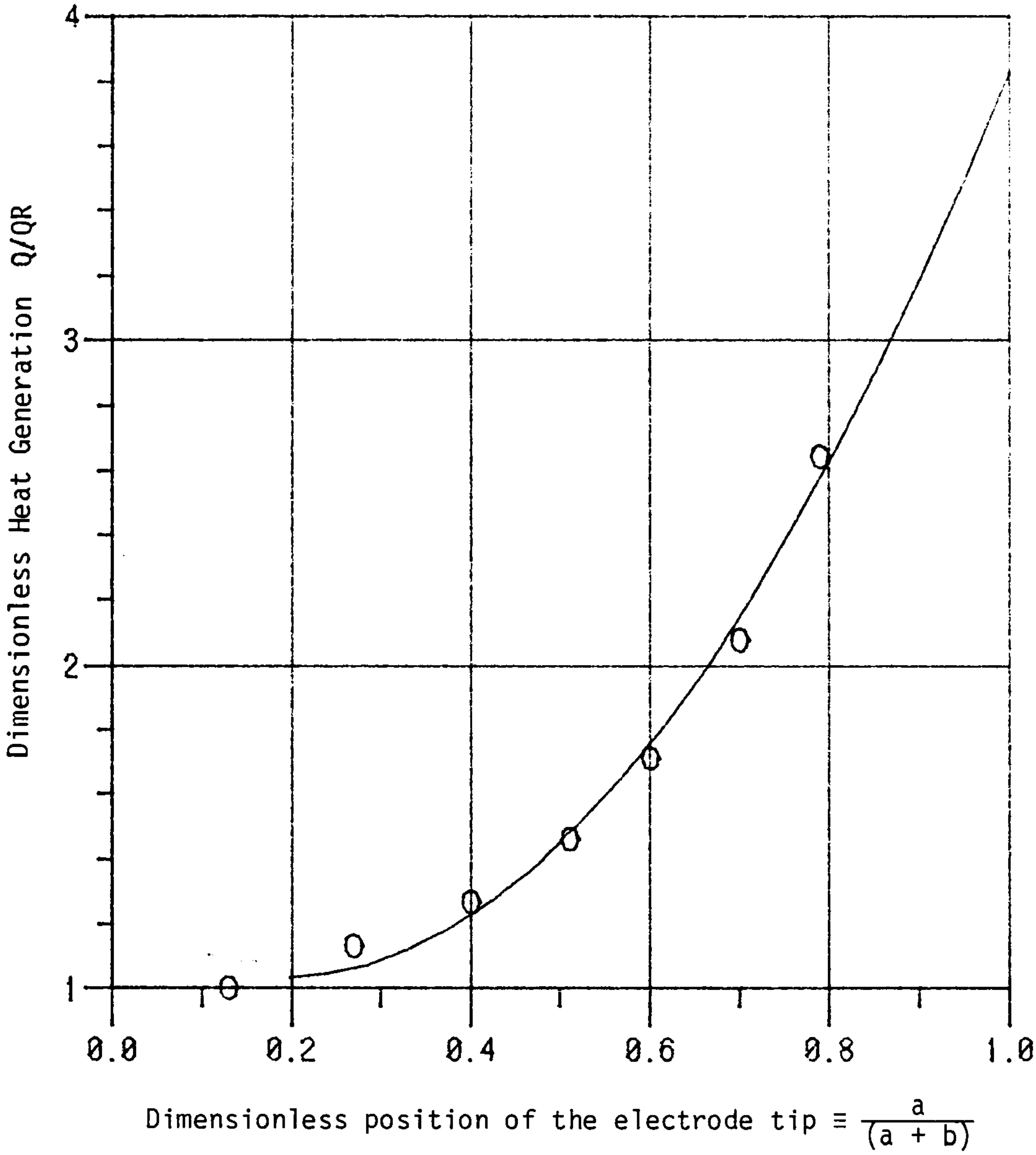

Figure 7. Relation Between Heat Generation and Electrode Penetration Depth, Q_R = 52 Kw (40 V, 1-3 KA)

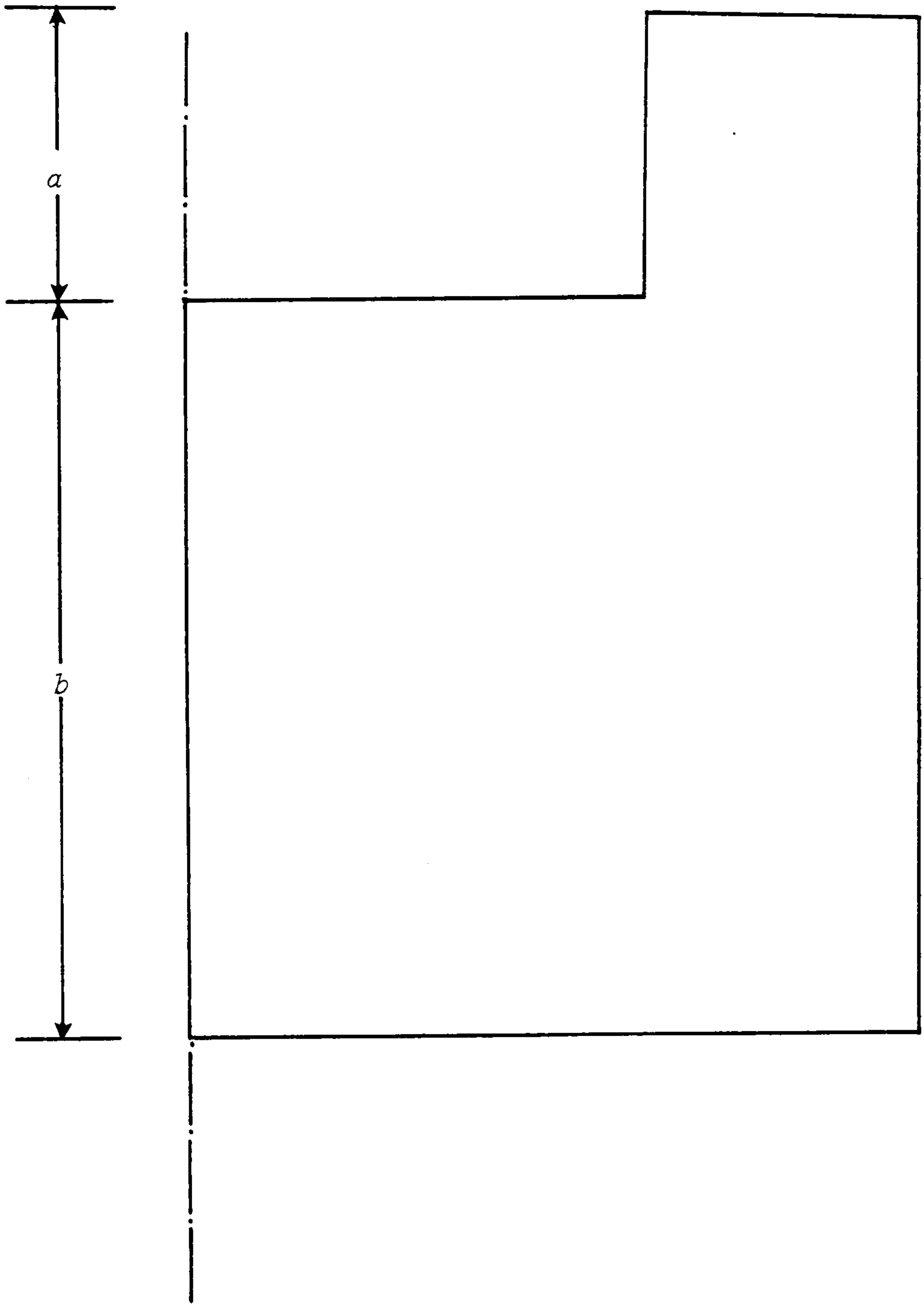

Figure 8. Distances *a* and *b* as Referred to in Figure 7 and Table 3

Temperature Distribution

The temperature distribution in the slag for operating condition 6 is shown in Figure 9. The temperature near the mold wall decreases (contour A, 1420°C) and becomes closer to the melting temperature of the slag due to the heat removal at the water channels. The maximum temperature (contour J, 1750°C) occurs under the electrode tip where most of the heat is generated. Mitchell et al[24] measured the temperature of the slag several millimeters below the electrode and reported a temperature of 1650°C. Mellberg[25] measured the temperature of the slag in a laboratory scale mold for an operating condition of 1.7 KA (AC), 39 V, as 1730°C at the center line near the slag-metal interface and 1800°C at 2.5 cm away from the center line.

The temperature distribution in the slag is shown in Figure 10 for a greater electrode penetration depth (operating condition 4). As discussed before, higher electrode penetration depth results in higher heat generation. These higher temperatures under the electrode would cause faster melting of the electrode. This shortens the electrode more rapidly and thereby tends to correct the excessive penetration. Conversely less electrode penetration results in lower temperatures in the slag. Therefore, it is to be noted that the electrode penetration depth is a function of the operating condition. This aspect of the process has not been modeled previously.

The reasonable temperature distribution in Figure 9 suggests that the electrode penetration depth in operating condition 6 is near the optimum for stabilized operation. The temperature distribution is shown in Figure 11 for the solid ingot and metal pool at operating condition 6.

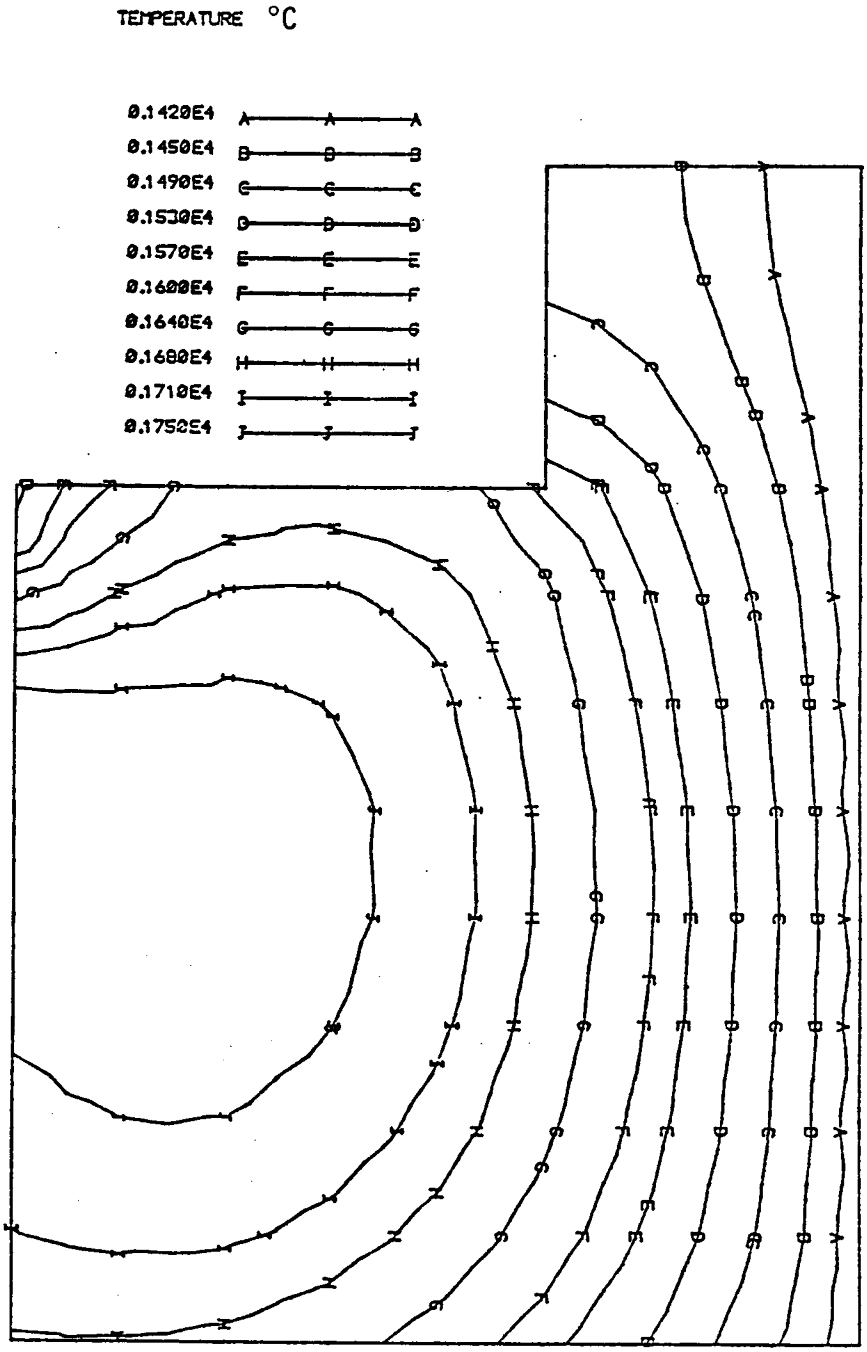

Figure 9. Temperature Distribution in the Slag for Operating Condition 6

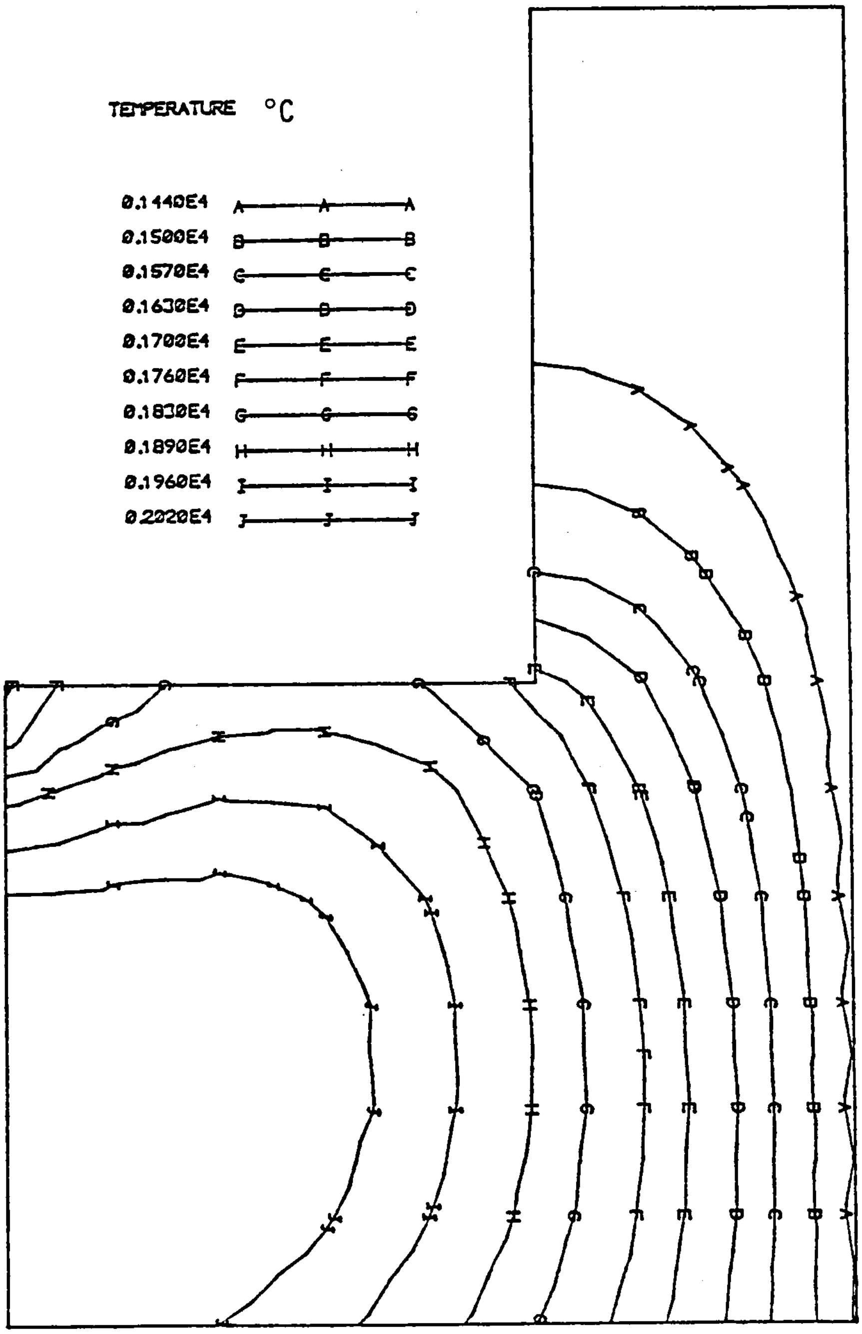

Figure 10. Temperature Distribution in the Slag for Operating Condition 4

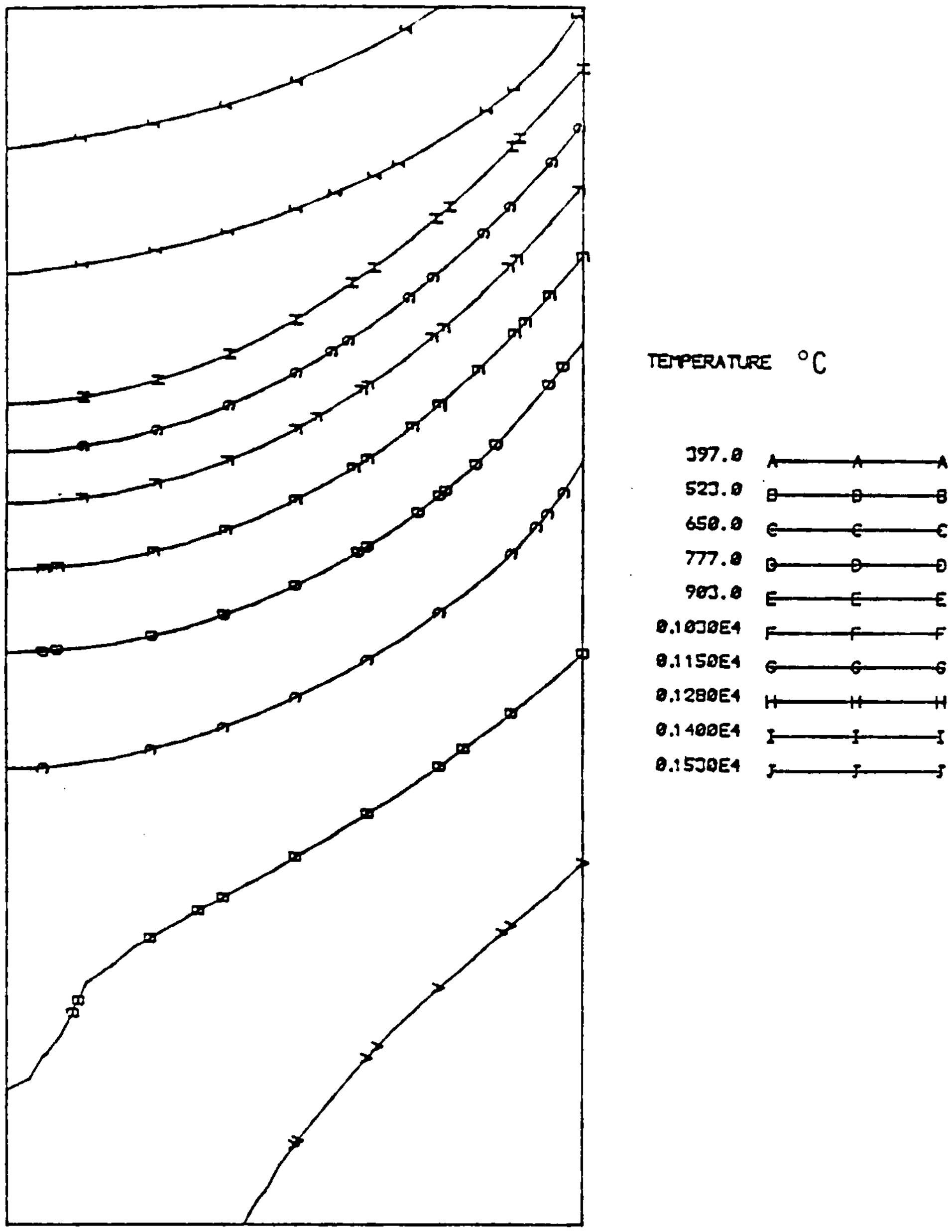

Figure 11. Temperature Distribution in the Metal Pool and Solid Ingot for Operating Condition 6

Here the boundary of the liquid metal pool, which is at 1450°C, is predicted by the model to be located next to contour I. The temperature distribution in the solid ingot and metal pool is shown in Figure 12 for the less than optimum operating condition 4. In this figure, the boundary of the metal pool is predicted to be located next to contour H. In this case, the figure suggests the maximum depth of the metal pool is approximately 5 cm. The more optimum condition in Figure 11 suggests a maximum metal pool depth of 2 cm. This is in good agreement with the theoretical finding of Choudhary and Szekely.[7] The relations between current and maximum metal pool depth as reported by them are in Figure 13. In this figure the solid line is their prediction and the dots are the predictions of this model.

In Figures 14 and 15 are the temperatures distributions in the mold wall at 4.2 mm away from the interior of the mold for operating conditions 6 and 4, respectively. In Figures 16 and 17 are the temperature distributions in the cross section of the mold wall for the above operating conditions.

These temperature distributions in the mold wall for the first time have been predicted by a comprehensive heat transfer model of the process. Figure 18 shows the temperature distribution in the mold wall as experimentally measured by Joshi and Mitchell[22] for an input power of 22.32 Kw (23.5 V, 0.95 A, AC) for a laboratory scale mold. Despite the difference in magnitude of the input power and the resulting temperatures between Figures 18 and 14, 15, there is good agreement in the general shape of the temperature profile and the location of different interfaces.

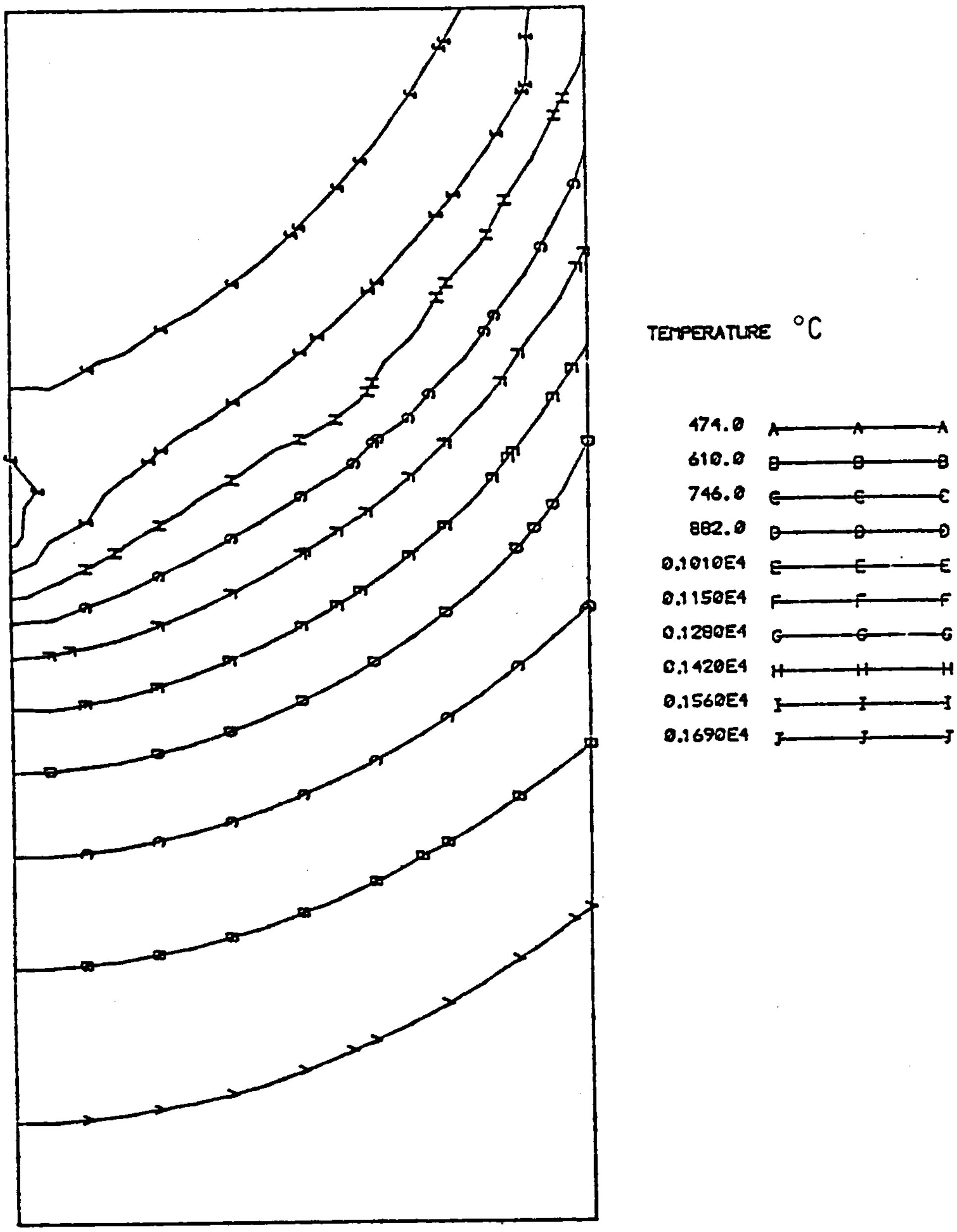

Figure 12. Temperature Distribution in the Metal Pool and Solid Ingot for Operating Condition 4

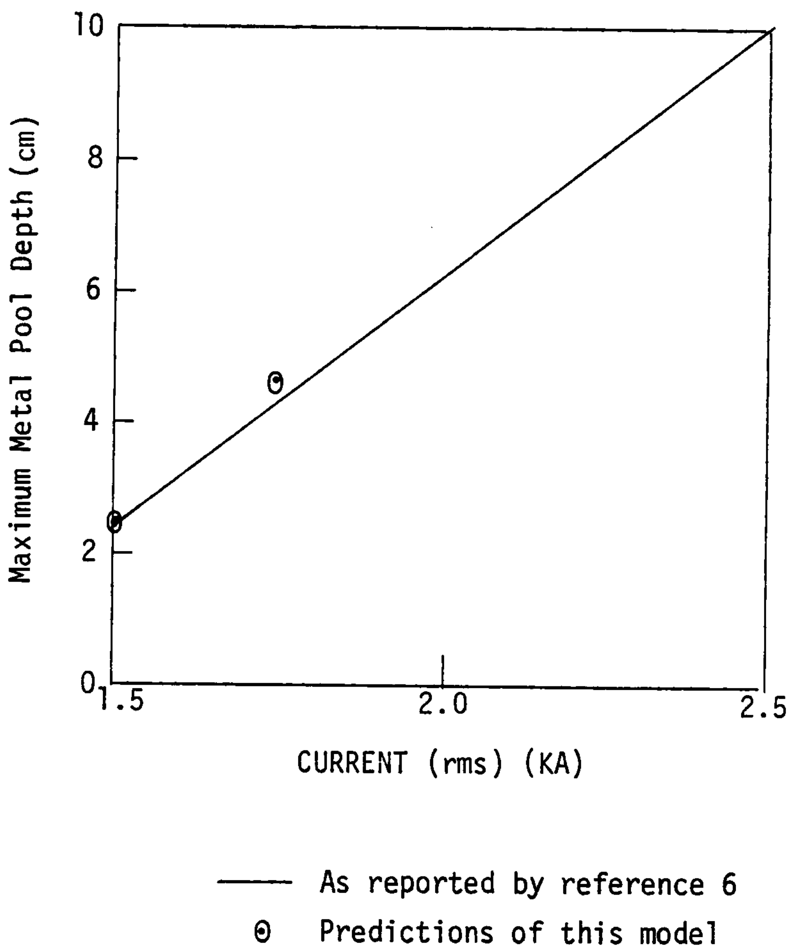

Figure 13. Relation between Current and Maximum Metal Pool Depth

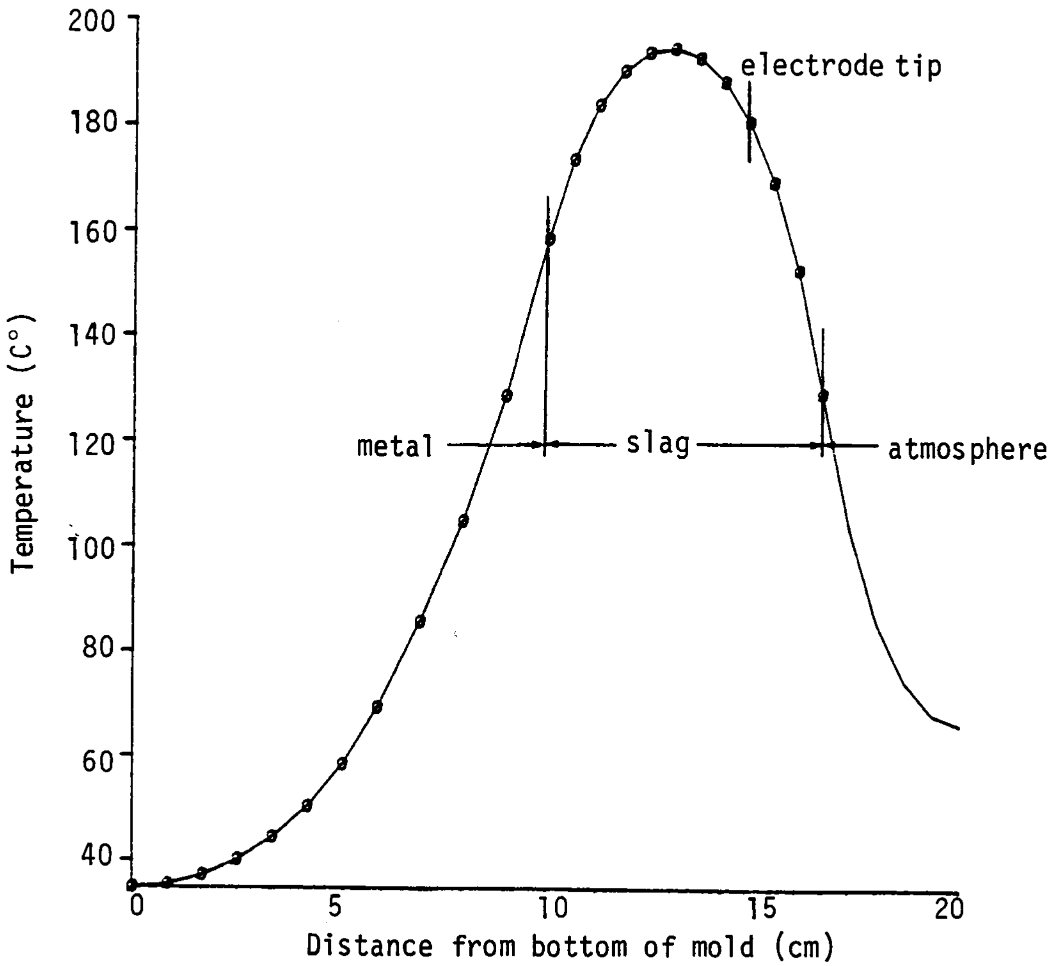

Figure 14. Temperature Profile in the Mold Wall at 4.2 mm away from the Interior of the Mold Wall for Operating Condition 6

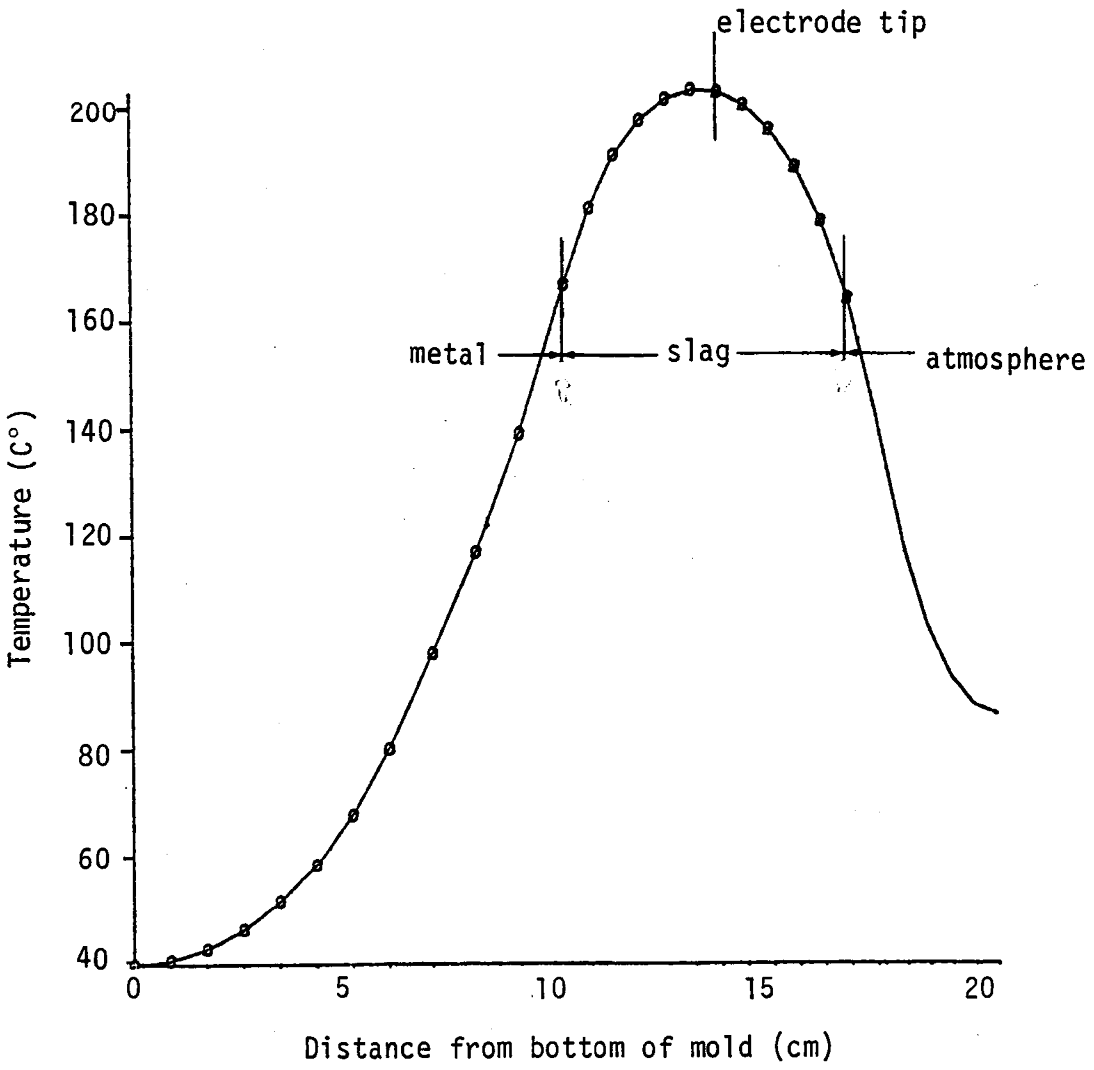

Figure 15. Temperature Profile in the Mold Wall at 4.2 mm away from the Interior of the Mold Wall for Operating Condition 4

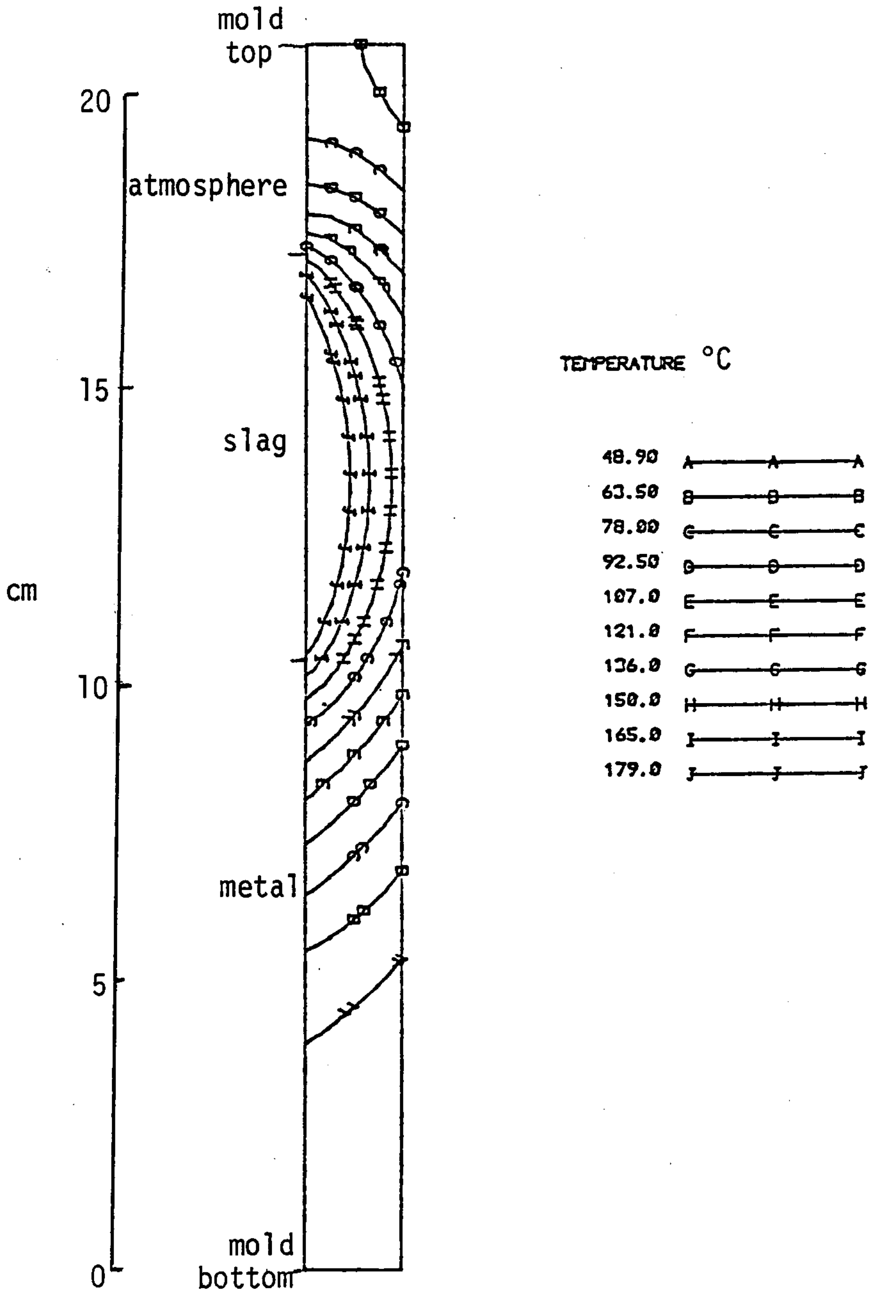

Figure 16. Temperature Distribution in the Cross Section of the Mold Wall for Operating Condition 6

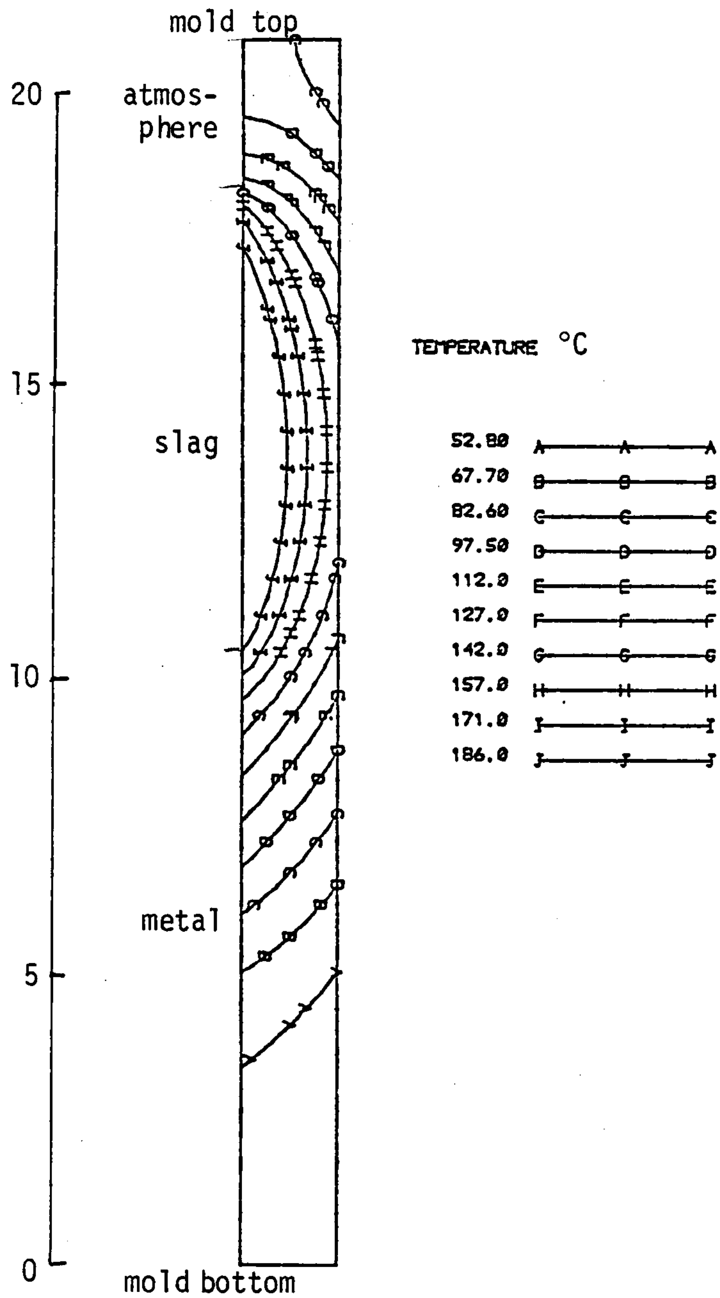

Figure 17. Temperature Distribution in the Cross Section of the Mold Wall for Operating Condition 4

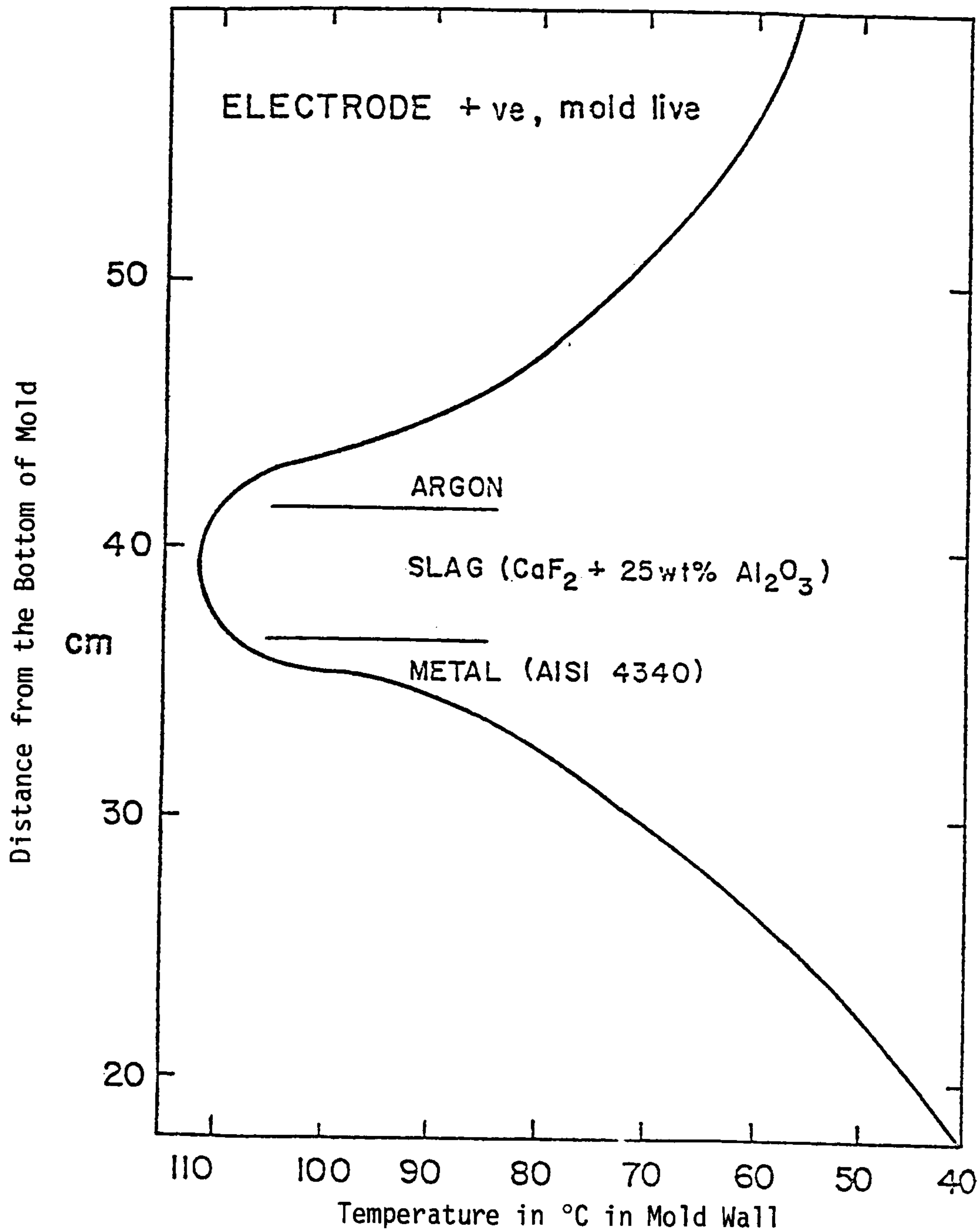

Figure 18. Temperature Profile in the Mold Wall Measured by Joshi and Mitchell[22] for Input Power of 22.3 W (23.5 V, 0.95 Amp) in a Laboratory Scale Mold

The mechanism of slag skin layer and air gap formation affects the temperature distribution in the mold wall.[26] Possible contact of molten metal with the mold wall at the slag-metal interface could result in a sharp temperature rise in the mold wall. Also melting or thinning of the skin layer by the liquid slag or ingot could result in temperature rises. On the other hand, thickening of the slag skin or air gaps could result in lowering the temperature in the wall. In this model, as explained before, allowance was made in the thermal conductivity of the skin layer at slag, metal pool, and solid ingot. Also a uniform thickness of the skin layer was considered at the above zones and the possibility of the contact of molten metal or slag with mold wall was not considered.

It is to be noted that for a more accurate representation of the temperature distribution in the mold wall, a combined analytical and experimental investigation is needed. The effective film coefficients would need to be measured experimentally for any particular operating condition.

6. CONCLUSIONS

A mathematical model of a prototypic collar mold for electroslag casting has been established with the governing equations for electric fields and heat transfer. Due to irregular geometry, solution by the finite element method is preferred. The first step in the solution was to determine the voltage distribution, which was then used for the calculation of heat generation. The resulting volumetric heat flux was then used as input for the finite element solution of the entire thermal field in the system. Features of the thermal model include the transfer of heat from the slag by metal droplets to the metal pool, the use of effective values of thermal conductivity to account for convection, and the use of melt rate as an imput parameter.

The results were compared with experimental results wherever possible; good agreement was observed. The predictive ability of the model in relating the input parameters to heat generation and temperature distributions leads to the following conclusions:

1. Most of the joule heating is under the electrode and heat generation becomes more uniform near the slag-metal interface.

2. The intensity and pattern of heat generation is very much affected by the geometry of the system.

3. For a fixed geometry and slag volume, both the heat generation and the molten slag temperature increase as the electrode penetration depth increases and visa versa.

4. The location of the maximum temperature of the slag is a few centimeters below the electrode center.

5. The temperature distribution in the mold wall was predicted by an overall heat transfer model of the process; this work had not been done in the references consulted.

6. The largest temperature rise in the mold wall is in the area of the molten slag. Therefore, the largest component of the heat transferred to the mold wall is from the molten slag.

7. The temperature profile in the mold wall is feasible for controlling the process. This has been demonstrated[1] experimentally, with the slag-metal interface location kept nearly constant through adjusting the ingot withdrawal rate.

On the basis of the foregoing, it is concluded that finite element modeling is a useful predictive tool for the electroslag casting process. Such models are recommended for design and modification of ESC systems such as, for example, when scaling up from a laboratory prototype casting system to a full-scale system. This work provides additional understanding about the collar mold which has been demonstrated[1] at ORNL for casting solid transition ingots.

However, the problem of producing hollow transition ingots has not received attention. Additional information relative to heat transfer characteristics of the center core is needed. The finite element approach here is well-suited for predictions of the performance of the hollow-ingot production process, and is a recommended approach in future research.

LIST OF REFERENCES

LIST OF REFERENCES

1. McEnerney, J. W., Dewey, B. R., Hutton, J. T., and David, D. S., System For Electroslag Casting Transition Ingots, ORNL TM-7548, Oak Ridge National Laboratory, 1980.

2. Stenzel, O. W., and Thomas, F. W., "Factors Influencing Slag and Metal Flow Patterns in ESR Furnaces," Proceedings of the Sixth International Conference on Special Melting, San Diego, CA, pp. 522-534, 1979.

3. Campbell, J., "Fluid Flow and Droplet Formation in the Electroslag Remelting Process," Journal of Metals, pp. 23-35, July 1970.

4. Dilawari, A. H., and Szekely, J., "A Mathematical Model of Slag and Metal Flow in the ESR Process," Metallurgical Transaction, Vol. 8B, pp. 227-236, June 1977.

5. Dilawari, A. H., and Szekely, J., Proceedings of the Fifth International Conference on Vacuum Metallurgy and Electroslag Refining Process, Munich, p. 157, 1976.

6. Dilawari, A. H., and Szekely, J., "Heat Transfer and Fluid Flow Phenomena in ESR," Metallurgical Transaction, Vol. 9B, pp. 77-86, March 1978.

7. Choudhary, M., and Szekely, J., "A Mathematical Model of Heat Transfer and Fluid Flow in ESR Process," Metallurgical Transaction, Vol. 11B, pp. 439-452, September 1980.

8. Kreyenberg, J., and Schwerdtfeger, K., "Stirring Velocities and Temperature Field in the Slag during Electroslag Remelting," Arch. Eisenhuttenwes, No. 1, Vol. 50, p. 1, 1979.

9. Inoue, M., and Iwasaki, T. (to be published, quoted in the paper by reference 10).

10. Kawakami, M., and Gogo, K. S., "A Survey on Profiles of Temperature and Electrical Potential in the Flux and Metal Pool During Electroslag Remelting," Proceedings of the Sixth International Conference on Special Melting, San Diego, CA, pp. 500-513, 1979.

11. Maulvault, M. A., "Temperature and Heat Flow in ESR," Ph.D. Thesis, Dept. of Met. and Mat. Sc., Mass. Inst. of Tech., 1971.

12. Duckworth, W. E., and Hoyle, G., Electroslag Refining, Chapman and Hall Ltd., London, 1969.

13. Sun, R. C., and Pridgeon, J. W., Second International Symposium on ESR, Mellon Inst., Pittsburgh, 1969.

14. Joshi, S., "The Thermal Characteristics of the Electroslag Remelting Process," Ph.D. Thesis, Dept. of Met., Univ. of British Columbia, 1971.

15. Carvajal, L. F., and Geiger, G. E., "An Analysis of the Temperature Distribution and the Location of the Solidus, Mushy, and Liquidus Zones for Binary Alloys in Remelting Processes," Metallurgical Transactions, Vol. 2, pp. 2087-2092, August 1971.

16. Elliot, J. F., and Maulvault, M., "Steady State Modelling of the ESR System," Proceedings of the Fourth International Symposium on ESR, Tokyo, pp. 69-80, 1963.

17. Mitchell, A., Szekely, J., and Elliott, J. F., "Applications of Mathematical Modelling to the ESR Process," Proceeding Conference on ESR, Sheffield, England, p. 3, 1973.

18. Paton, B. E., Medovar, B. I., Kozlitin, D. A., Emelyanenko, Yu. G., Sterebogenand, Yu. A., and Baglai, V. M., "Mathematical Simulation and Prediction of Electroslag Refining of Large Forging Ingots," Proceeding Conference on ESR, Sheffield, England, p. 16, 1973.

19. Basaran, M., Mehrabian, R., Kattamis, T. Z., and Flemings, M. C., "A Study of the Heat and Fluid Flow in ESR," Mass. Inst. of Tech., AD-782 228, 1974.

20. Paton, B. E., Modovar, B. I., Demchenko, V. F., Khorungy, J. G., Shevtozov, V. L., Shatanko, A. G., and Bogachenko, "Calculation of Temperature Fields in Plate Ingots and in Ingot-Slabs of ESR," Proceedings of the Fifth International Symposium on ESR, Carnegie-Mellon Univ., pp. 323-344, 1974.

21. Ballantyne, A. S., and Mitchell, A., "Modelling of Ingot Thermal Fields in Consumable Electrode Remelting Processes," Ironmaking and Steelmaking, No. 4, pp. 222-239, 1977.

22. Joshi, S., and Mitchell, A., "Heat Flow in the Electroslag Process," Proceedings of the Third International Symposium on ESR, Carnegie-Mellon Univ., Part 1, pp. 27-52, 1971.

23. Roy, T. Deb, Szekely, J., and Eagar, T. W., "Heat Generation Patterns and Temperature Profiles in Electroslag Welding," Mass. Inst. of Tech., 1980.

24. Mitchell, A., Joshi, S., and Cameron, J., "Electrode Temperature Gradients in the Electroslag Process," Metallurgical Transaction, Vol. 2, pp. 561-567, February 1971.

25. Mellberg, P. O., "Temperature Distribution in Slag and Metal During Electroslag Remelting of Ball-Bearing Steel," Proceedings of the Fourth International Symposium on ESR, Tokyo, pp. 13-25, 1973.

26. Hoyle, G., "Surface Phenomena in ESR," Proceedings of the Sixth International Conference on Special Melting, San Diego, CA, pp. 624-640, 1979.

27. PAFEC 75 Data Preparation, PAFEC, Lt., Nottingham, UK, 1978.

28. Dewey, B. R., and Lagerberg, G., Analytical Studies of Collar Mold for Electroslag Casting, ORNL/Sub-7685/1, Department of Engineering Science and Mechanics, University of Tennessee, Knoxville, 1980.

29. Pressure Vessel and Piping, 1972 Computer Programs Verification, ASME, New York, NY, 1972.

VITA

Shahab Hatamtabrizi was born in Tehran, Iran on June 7, 1958. He attended elementary and high schools in that city and was graduated from Paymen high school in 1975. In fall 1976 he entered Oscar Rose Junior College, and transferred to the University of Tennessee, Knoxville in June of 1978, and in June of 1980 he received a Bachelor of Science degree in Mechanical Engineering.

In September of 1980, Mr. Hatamtabrizi entered the Graduate School of the University of Tennessee, Knoxville; he received the Master of Science degree with a major in Engineering Science in December of 1981.

The author is a member of the American Society of Mechanical Engineers. Mr. Hatamtabrizi has accepted a teaching assistantship at The University of Tennessee, Knoxville, in the fall of 1981, and has applied for admittance to the doctoral program in the Department of Engineering Science and Mechanics, The University of Tennessee.